Effect of improving representation of horizontal and vertical cloud structure on the Earth's global radiation budget. Part II: The global effects

RMetS
Royal Meteorological Society

Effect of improving representation of horizontal and vertical cloud structure on the Earth's global radiation budget. Part II: The global effects

Jonathan K. P. Shonk*and Robin J. Hogan
Department of Meteorology, University of Reading, UK
*Correspondence to: Jonathan Shonk, Department of Meteorology, University of Reading, Earley Gate, Reading RG6 6BB, Berkshire, UK. E-mail: j.k.p.shonk@reading.ac.uk

Reliably representing both horizontal cloud inhomogeneity and vertical cloud overlap is fundamentally important for the radiation budget of a general circulation model. Here, we build on the work of Part I of this two-part paper by applying a pair of parametrizations that account for horizontal inhomogeneity and vertical overlap to global re-analysis data. These are applied both together and separately in an attempt to quantify the effects of poor representation of the two components on radiation budget.

Horizontal inhomogeneity is accounted for using the 'Tripleclouds' scheme, which uses two regions of cloud in each layer of a gridbox as opposed to one; vertical overlap is accounted for using 'exponential-random' overlap, which aligns vertically continuous cloud according to a decorrelation height. These are applied to a sample of scenes from a year of ERA-40 data. The largest radiative effect of horizontal inhomogeneity is found to be in areas of marine stratocumulus; the effect of vertical overlap is found to be fairly uniform, but with larger individual short-wave and long-wave effects in areas of deep, tropical convection. The combined effect of the two parametrizations is found to reduce the magnitude of the net top-of-atmosphere (TOA) cloud radiative forcing by 2.25 W m^{-2}, with shifts of up to 10 W m^{-2} in areas of marine stratocumulus.

The effects on radiation budget of the uncertainty in our parametrizations is also investigated. It is found that the uncertainty in the impact of horizontal inhomogeneity is of order $\pm$ 60%, while the uncertainty in the impact of vertical overlap is much smaller. This suggests an insensitivity of the radiation budget to the exact nature of the global decorrelation height distribution derived in Part I.

Key Words: cloud inhomogeneity; overlap; decorrelation height; Tripleclouds; exponential-random.

Received 13 July 2009; Revised 31 March 2010; Accepted 12 April 2010; Published online in Wiley InterScience 23 July 2010

Citation: Shonk JKP, Hogan RJ. 2010. Effect of improving representation of horizontal and vertical cloud structure on the Earth's global radiation budget. Part II: The global effects. *Q. J. R. Meteorol. Soc.* **136**: 1205–1215. DOI:10.1002/qj.646

1. The Tripleclouds scheme

Clouds are recognised as a major source of uncertainty in climate models (Randall, *et al.*, 2007). It is therefore imperative that parametrizations of cloud properties describe the cloud and its processes as realistically as possible. However, most radiation schemes in general circulation models (GCMs) represent clouds as plane-parallel and align them using maximum-random overlap, whereby vertically continuous clouds are overlapped maximally and clouds

separated by layers of clear sky are overlapped randomly. The use of these approximations causes large, systematic biases in the radiative fluxes above and below the clouds (e.g. Barker, *et al.*, 1999; Carlin, *et al.*, 2002).

Shonk and Hogan (2008) introduced a new cloud representation scheme, referred to as 'Tripleclouds', that improves on the conventional plane-parallel cloud scheme by partitioning the cloud in each layer of a gridbox into two homogeneous regions of equal fractional area. One of these regions contains the optically thinner half of the cloud in that layer; the other contains the optically thicker half. A third region contains the clear sky. The two values of water content for the cloudy regions are defined to approximately represent the standard deviation of water content in the layer. In an operational GCM, the standard deviation could either be specified using an empirical value or, in some recent schemes, taken from an explicit representation of variance (e.g. Tompkins, 2002). A review of a number of studies by Shonk, *et al.* (2010), hereafter 'Part I', sought to quantify this spread in terms of fractional standard deviation, defined as the quotient of the standard deviation of water content and its mean:

$$f_w = \frac{\sigma_w}{\overline{w}} . \tag{1}$$

We found f_w to be 0.75 ± 0.18, with no systematic dependence on cloud type, observation type or gridbox size. Tripleclouds was implemented in the Edwards–Slingo radiation code (Edwards and Slingo, 1996), and tests using radar data scenes in Part I showed that significant additional biases are not introduced into the radiation fields when using this mean value, and a mean plane-parallel bias in cloud radiative forcing (CRF) of 8% could be reduced to less than 1% using Tripleclouds.

Hogan and Illingworth (2000) proposed an overlap scheme that we refer to as 'exponential-random' overlap, where vertically continuous cloud is overlapped not maximally or randomly, as in all previous schemes, but according to an 'overlap parameter', α, whose value varies from zero for random overlap to one for maximum overlap. They found the value of α to decay roughly inverse-exponentially with layer separation for layers within vertically continuous clouds, over a decorrelation scale of order 1.5 km for a midlatitude location. In Part I, we combined this with results from the cloud radar measurements of Mace and Benson-Troth (2002) to derive a simple latitudinal relationship for this decorrelation scale. We introduced a slightly different form of overlap parameter, β, with a definition that allowed exponential-random overlap to be applied to three-region systems as well as two-region systems. We converted the α decorrelation scales of Hogan and Illingworth (2000) and Mace and Benson-Troth (2002) to β decorrelation scales and found the best-fit latitude relationship to be:

$$Z_{0\beta} = 2.174 - 0.0207\phi , \tag{2}$$

where $Z_{0\beta}$ is decorrelation height in kilometres and ϕ is absolute latitude in degrees. Seasonal effects were found to cause a variation of order ± 0.5 km in $Z_{0\beta}$. For a three-region system with one clear-sky region and two cloudy regions, a decorrelation height of $Z_{0\beta}$ is applied to the clear-sky region only and a height of $Z_{0\beta}/2$ is applied to the cloudy regions. This choice is based on the results of Räisänen, *et al.* (2004), within the limitations discussed in Part I.

In this paper, we combine Tripleclouds with exponential-random overlap and apply it to the European Centre for Medium-Range Weather Forecasts (ECMWF) re-analysis (ERA-40) data to investigate the impact of cloud structure on the global radiation budget for a realistic distribution of clouds. The individual radiative effects of the modification of horizontal inhomogeneity and vertical overlap are investigated and compared. The method used to investigate these contributions is discussed in section 2. In section 3, the radiation calculations are performed and the global radiation budget from our ERA-40 data compared with radiation budget measurements derived from the Clouds and the Earth's Radiant Energy System (CERES) project. The individual effects of the horizontal and vertical components of the Tripleclouds scheme are considered, along with the total effects, in section 4, both in terms of radiation and cloud cover. Finally, the paper is concluded in section 5.

2. Data and experimental method

The global data used in this investigation are extracted from the ERA-40 re-analysis dataset. Compiled by the ECMWF (Uppala, *et al.*, 2005), ERA-40 is a global dataset of meteorological variables stored at six-hourly intervals over the 45-year period from September 1957 to August 2002. Its available cloud variables consist of separate fields of ice water content, liquid water content and cloud fraction. These are taken directly from the model, with no assimilated cloud observations, on a grid with resolution of $1.125^\circ \times 1.125^\circ$. This equates to a gridbox size of 110 km at the Equator and about 60 km at midlatitudes (and a global average gridbox size of order 85 km). The data are stored on 60 vertical levels, extending from the surface up to a pressure of 10 Pa.

A single year of the ERA-40 dataset is used. As the variety and quality of data sources assimilated into the re-analysis increases throughout the 45-year time period, we choose 2001, the most recent full year available. From this year of data, we extract January, April, July and October to give a sample of the weather in each season. This gives us a set of 480 scenes: four scenes for each of the first 30 days of each of the four months, at 0000, 0600, 1200 and 1800 UTC each day.

However, using only four scenes per day for short-wave radiative transfer calculations leads to the complication that, for any given location, the calculation is only performed with the sun above the horizon at two solar zenith angles. This could lead to systematic localised errors in flux calculations. In the interests of minimising these systematic errors without drastically increasing radiation calculation time, the choice is made to increase the number of scenes per day to eight, giving a three-hour temporal resolution. This is achieved by recalculating the radiative transfer for the same cloud fields, but using a solar zenith angle field that has been advanced by three hours. In a simple, idealised test, this was seen to reduce local errors in cloud radiative forcing from up to 20% to less than 5%.

As in Part I, the radiative transfer calculations are performed using the Edwards–Slingo radiation code (Edwards and Slingo, 1996). For all calculations, constant effective radius values of 30 μm and 10 μm are used for ice particles and liquid droplets respectively. Ice particles are treated as spheres in the long-wave calculation; in the short-wave, the parametrization of Kristjánsson, *et al.* (2000) is employed. The global distribution of short-wave surface

Table I. List of the cloud representations applied to global scenes of ERA-40 in this experiment, with their abbreviations.

Experiment code	Description	f_w	$Z_{0\beta}$ (km)
Plane-parallel, single-column representations			
clear	Clear-sky calculation to enable derivation of CRFs.	0	∞
PPm	Calculation using maximum-random overlap.	0	∞
Tripleclouds, single-column representations			
TCm	Calculations using maximum-random overlap.	0.75	∞
TCm_+	As TCm, but with greater horizontal inhomogeneity.	0.93	∞
TCm_-	As TCm, but with less horizontal inhomogeneity.	0.57	∞
TCe	Calculations using exponential-random overlap.	0.75	$2.174 - 0.0207\phi$
TCe_+	As TCe, but with more maximum overlap.	0.75	$2.666 - 0.0232\phi$
TCe_-	As TCe, but with more random overlap.	0.75	$1.894 - 0.0172\phi$

f_w is the water content fractional standard deviation used in the Tripleclouds calculations.
$Z_{0\beta}$ is the equation of decorrelation height used in exponential-random overlap calculations.

albedo from the ERA-40 data is used, with a single albedo value at each grid point that applies to the whole short-wave spectrum. The long-wave surface emissivity is set to a constant global value of 0.98. We use well-mixed profiles of oxygen, carbon dioxide, methane, nitrous oxide, CFC-11 and CFC-12, with mixing ratios that are typical, present-day values. A profile of ozone mass mixing ratio is taken from the midlatitude summer atmosphere (McClatchey, *et al.*, 1972). Water vapour distributions are derived from ERA-40; aerosols are not used in the calculations. The calculations divide the short-wave part of the spectrum into five bands and the long-wave part into nine bands.

Four radiative transfer calculations are performed on each scene: a clear-sky calculation to enable calculation of cloud radiative forcing; a baseline calculation using plane-parallel clouds and maximum-random overlap (PPm); a further maximum-random overlap calculation but with Tripleclouds applied (TCm); and a calculation with Tripleclouds combined with exponential-random overlap (TCe). Tripleclouds is applied to each layer of each scene of ERA-40 data using the 'fractional standard deviation method': the pair of values of water content for Tripleclouds, w_{TC}, is calculated from the single mean water content value stored in the dataset, $\overline{w}$, using the fractional standard deviation $f_w = 0.75$ as determined in Part I via:

$$w_{\mathrm{TC}} = \overline{w} \pm f_w \overline{w} \,. \tag{3}$$

In the event of mixed-phase clouds occurring, this equation is applied separately to the ice and liquid cloud water contents. Exponential-random overlap is applied using the derived variation of the decorrelation height $Z_{0\beta}$ with latitude stated in (2). The cloud configurations used in this experiment are shown by the schematics in Figure 1 for a single pair of cloudy layers. For completeness, a schematic of exponential-random overlap with plane-parallel clouds is shown (PPe), although radiative calculations using this configuration are not performed.

The performance of the representations are compared in terms of improvements in TOA and surface cloud radiative forcing (CRF). As the changes in CRF are an attempt to offset the plane-parallel biases, we shall refer to them throughout this study as 'shifts' as opposed to 'biases'. We evaluate the improvement in radiation budget that is due to the inclusion of horizontal inhomogeneity (the 'horizontal shift') as the difference between the PPm and TCm results

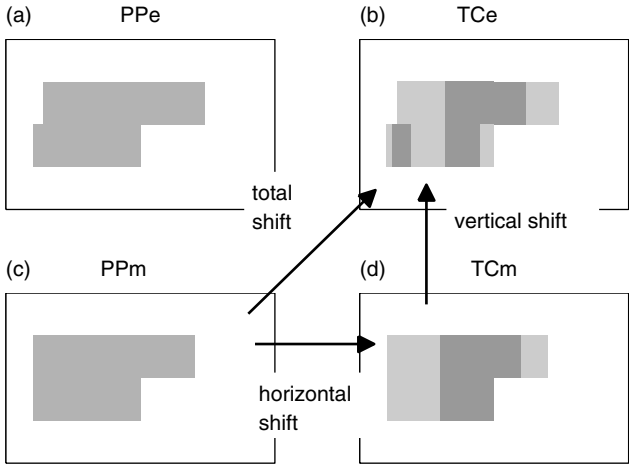

Figure 1. Schematic of the cloud representations described in Table I, using a pair of cloud layers with cloud fractions of 0.6 and 0.4 in the upper and lower layers respectively. Note that the PPe configuration is shown here only for completeness; it is not used in the experiment. The changes in cloud approximation that give the CRF 'shifts' (see text) are shown by the arrows.

and the improvement that is due to vertical overlap (the 'vertical shift') as the difference between the TCm and TCe results. This choice results in the combined change in CRF (the 'total shift') then being equal to the sum of these two shifts, and also the difference between the PPm and TCe results. The pairs of cloud approximations used to determine our CRF shifts are indicated by the arrows in Figure 1.

We also investigate the effects on radiation budget of the uncertainty in our horizontal and vertical cloud structure parametrizations by performing additional radiative transfer calculations on a sample of the scenes. We perform extra calculations using the TCm representation with $f_w = 0.57$ and $f_w = 0.93$ (the upper and lower error bar values of f_w identified in Part I), so that we can generate error bars on our horizontal shift by comparing PPm results with TCm_+ and TCm_- (Table I). The effect of vertical overlap uncertainty is investigated by applying fits of $Z_{0\beta}$ for the upper and lower limits of the error bars in Figure 4 of Part I. (The equations for these fits are given in Table I.) Error bars in CRF are then generated by comparing the unperturbed TCm CRFs with those from TCe_+ and TCe_-. The errors in total CRF are determined by adding the horizontal and vertical shift

errors in quadrature, using the assumption that they are independent of each other.

3. Global radiation budget

The first step of the experiment seeks to verify that the CRFs calculated using the ERA-40 data in the Edwards–Slingo radiation code are realistic by comparing them with measurements from the CERES project (Wielicki, *et al.*, 1996). We calculate mean global distributions of TOA short-wave and long-wave CRF over the four months of the ERA-40 data using the original plane-parallel, maximum-random cloud scheme (PPm) and the new Tripleclouds scheme with exponential-random overlap (TCe). These mean CRFs are compared with mean TOA CRFs for the same four months extracted from CERES data in Figure 2. Figures 2(a, b) show the CERES radiation budget, and (c, d, e, f) the differences between these and the CRFs calculated from ERA-40. Zonal averages of the CRF distributions used in Figure 2 are shown separately in Figure 3; the global mean CRFs are given in Table II.

It is seen that our calculated global average short-wave CRF using TCe agrees with the CERES value to within $1\,\mathrm{W\,m^{-2}}$. Despite this, the local errors are large in places, with a general tendency for our ERA-40 short-wave CRFs to be too large in magnitude over the tropical ocean and too small in magnitude at higher latitudes. A similar result was found by Allan, *et al.* (2004). They attributed the differences to issues with the occurrence of clouds in ERA-40, discussed by Chevallier, *et al.* (2001). The tendency for short-wave CRF biases to be positive at mid-to-high latitudes and negative in the Tropics is also evident on Figure 3. The magnitudes and signs of these latitudinally averaged biases agree with the results of Bender, *et al.* (2006), who compared radiation budgets from a number of GCMs with observed budgets from CERES and the Earth Radiation Budget Experiment (ERBE).

Globally, long-wave CRFs are found to be too low in magnitude by about $7\,\mathrm{W\,m^{-2}}$ with respect to CERES. We clearly see this effect in the long-wave in Figure 3, with a bias of order $10\,\mathrm{W\,m^{-2}}$ in the midlatitudes. This difference is much larger than the changes in the ERA-40 radiation budget made by applying Tripleclouds, and is partly due to the fact that CERES clear-sky fluxes are only measured in locations of clear sky. In fact, there are a few locations where CRF data are unavailable, mostly at high latitudes (shown by the dark patches). This is because clear-sky conditions do not occur here at the time of a satellite overpass. Ideally, values of CRF should be calculated by comparison of a radiative calculation in the presence of clouds with a calculation using the same profile of water vapour in the absence of clouds. In practice, however, the water vapour profile of observed

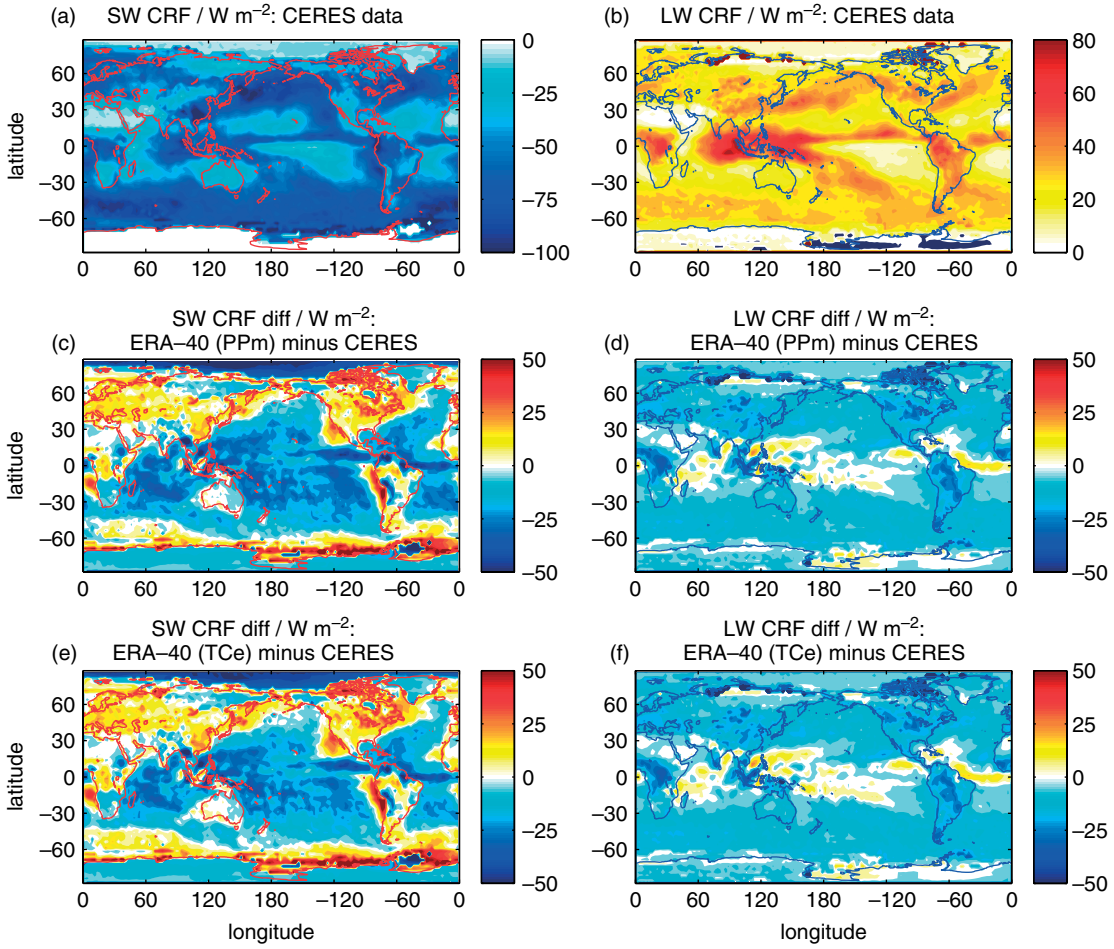

Figure 2. Comparison of global radiation budget in terms of top-of-atmosphere cloud radiative forcing (CRF). (a) and (b) show the average CERES measurements from 2001; (c) and (d) show the calculated CRFs from ERA-40 when clouds are represented using a plane-parallel, maximum-random (PPm) scheme; (e) and (f) show CRFs when using Tripleclouds with exponential-random overlap. (c) to (f) are expressed as differences from the CERES values. Missing CERES data at high latitudes are shown by the dark patches. (a, c, e) show short-wave CRFs; (b, d, f) long-wave CRFs.

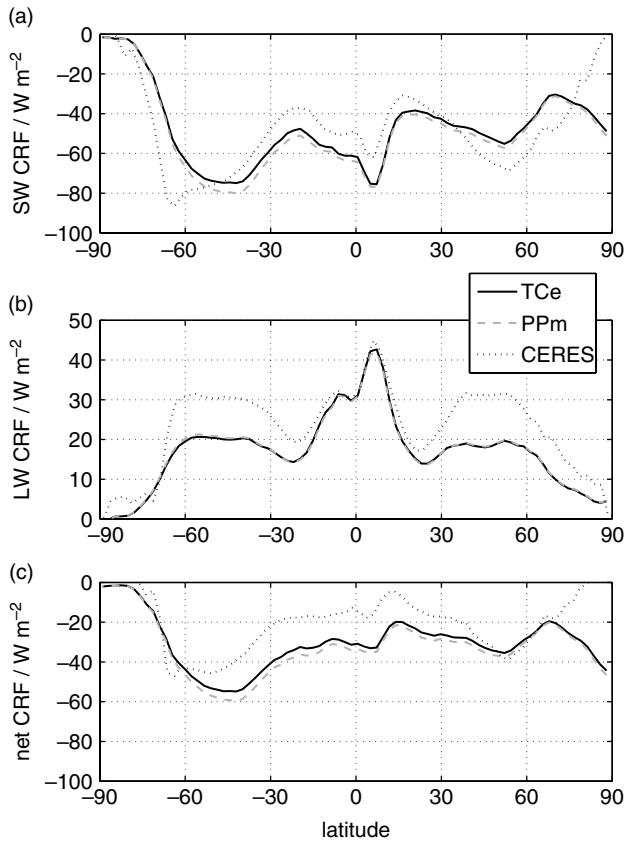

Figure 3. Variation of zonal mean values of (a) short-wave, (b) long-wave and (c) net top-of-atmosphere cloud radiative forcing (CRF). CRFs calculated from the year of ERA-40 are shown for two of the cloud schemes (PPm and TCe) by the solid and dashed lines; the CRFs from CERES for the same period is shown by the dotted line.

Table II. Global means of cloud radiative forcing (CRF, W m^{-2}) at the top of the atmosphere (TOA) taken from CERES and calculated from ERA-40 using different cloud representations. Abbreviations for cloud representations are defined in Table I.

	TOA SW	TOA LW	TOA net
CERES CRF	−46.93	23.81	−23.12
PPm CRF	−49.72	16.94	−32.78
TCe CRF	−47.43	16.90	−30.53

clear-sky areas tends to be systematically drier. In the long-wave, this deficit of water vapour is found to result in CERES outward clear-sky fluxes that are too large in regions of warm ascent by up to 15 W m^{-2} (Allan and Ringer, 2003).

Some local differences between the CRF fields are also seen over land surfaces in the tropics, particularly in the long-wave. In the CERES data, there are patches of higher long-wave CRF over northern South America and central Africa, with values of over 60 W m^{-2}. In the long-wave CRFs calculated from ERA-40, values in these locations are lower by about 25 W m^{-2}. This suggests fundamental differences in the clouds measured during CERES and the modelled clouds used in ERA-40, most notably the implication that deep, tropical convection is poorly represented by the model, particularly over land. Even so, a comparison of ECMWF model cloud output with radar data from three Cloudnet sites in Europe by Illingworth, *et al.* (2007) revealed a fair agreement in depictions of ice water content and liquid water content. Also, Chevallier, *et al.* (2001) found both the global distribution and seasonal cycle of cloud in the ERA-40 dataset to be realistic, although with a few shortcomings identified. It should be re-emphasised that the clouds present in ERA-40 are extracted directly from the ECMWF model and constrained using data assimilation: no cloud observations were directly used in the dataset. This means that the clouds in ERA-40 take the same form as GCM clouds, which is ideal for our experiments. While we accept that there may be a few shortcomings in the ERA-40 cloud fields with respect to reality, we shall make use of them for this investigation.

4. Global effect of cloud structure

In this section, we first consider changes in global cloud cover calculated from the ERA-40 data, averaged over the four months (Figure 4). We then use the method discussed at length in section 2 to evaluate the changes to the global radiation budget caused by the individual implementation of Tripleclouds and exponential-random overlap, and also their combined effects. The global distributions of these CRF shifts are shown in Figures 5, 6 and 7. Each figure shows the mean distribution of short-wave, long-wave and net CRF shift averaged over the year. Global mean shifts, with error bars caused by the uncertainty in our parametrizations of f_w and $Z_{0\beta}$, are given in Table III. The sizes of the error bars are stated as pairs of numbers, as the upper and lower bounds are found to not be equally spaced from the mean value. The shifts are also shown averaged zonally in Figure 9, again with error bars.

4.1. *Effect of vertical structure on cloud cover*

We first consider the effects of our new vertical overlap scheme on global cloud cover, which is one of the most important mechanisms by which clouds affect radiation budget (Slingo, 1990). Cloud cover is calculated for each ERA-40 scene using maximum-random, exponential-random and random overlap, then averaged to give a mean over the whole period. It is unimportant which horizontal structure scheme is used as, by definition, the Tripleclouds scheme does not affect cloud fraction in individual layers and will have no effect on cloud cover.

The global distribution of cloud cover when maximum-random overlap is applied is presented in Figure 4(a); the increase in cloud cover when exponential-random overlap is implemented is shown in Figure 4(b). High cloud cover is found in the storm tracks, where deep, structured cloud is often present. In these locations, we also find the largest shifts in cloud cover, up to an increase of 0.1. In the Tropics, the prevalence of high-level convective anvils also give a cloud cover of near 1, although their lesser vertical extent leads to a much smaller vertical shift in cloud cover. The effect of using exponential-random overlap is to increase the cloud cover in all locations where clouds exist.

A similar study of overlap on ECMWF model data was performed by Morcrette and Jakob (2000). The global distribution of cloud cover in our Figure 4 is similar to their Figure 3 and our vertical shifts between maximum-random and random overlap (not shown) similar to their Figure 4, although the sign of their shift is sometimes negative. This

Table III. Global mean shifts in CRF ($W\,m^{-2}$) when the cloud horizontal and vertical structure representations are improved. Abbreviations for cloud representations are defined in Table I. The error bars represent the effect of applying different fractional standard deviations and overlap decorrelation heights as shown in Table I.

	TCm−PPm (horizontal shift)	TCe−TCm (vertical shift)	TCe−PPm (total shift)
Top-of-atmosphere			
Short-wave	$6.15\ (^{+5.91}/_{-3.03})$	$-3.86\ (^{+0.61}/_{-0.23})$	$2.29\ (^{+5.94}/_{-3.05})$
Long-wave	$-2.02\ (^{+1.01}/_{-2.10})$	$1.98\ (^{+0.09}/_{-0.25})$	$-0.04\ (^{+1.02}/_{-2.11})$
Net	$4.13\ (^{+3.81}/_{-2.02})$	$-1.88\ (^{+0.36}/_{-0.14})$	$2.25\ (^{+3.83}/_{-2.03})$
Surface			
Short-wave	$6.66\ (^{+6.24}/_{-3.27})$	$-4.11\ (^{+0.64}/_{-0.24})$	$2.56\ (^{+6.27}/_{-3.23})$
Long-wave	$-2.89\ (^{+1.57}/_{-4.05})$	$2.18\ (^{+0.13}/_{-0.40})$	$-0.70\ (^{+1.58}/_{-4.07})$
Net	$3.77\ (^{+2.18}/_{-1.69})$	$-1.92\ (^{+0.23}/_{-0.11})$	$1.85\ (^{+2.54}/_{-1.79})$

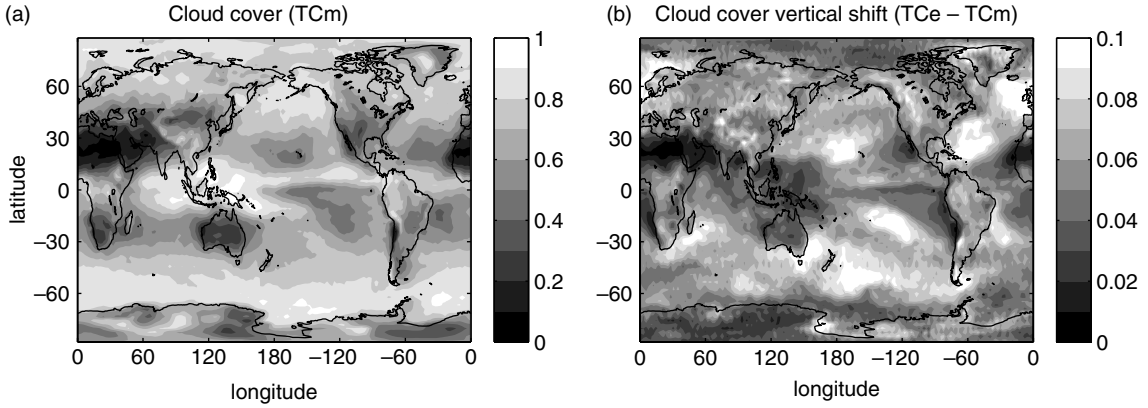

Figure 4. Cloud cover calculated from the year of ERA-40 data using different cloud overlap approximations. (a) shows the cloud cover when the cloud is overlapped using maximum-random overlap; (b) shows the shift in cloud cover introduced by replacing maximum-random overlap with exponential-random. The global effect of improving the overlap assumption is to increase the global mean cloud cover from 0.660 to 0.716.

is because their study implemented the overlap schemes in the radiation code and performed a short model integration using the overlap scheme interactively. We find an increase in mean global cloud cover from 0.660 to 0.716 when exponential-random overlap is performed, and to 0.786 when random overlap is performed. Our vertical shift to random overlap is greater in size than that of Morcrette and Jakob (2000), whose cloud cover rose from 0.639 to 0.708. This difference is attributable to differences in vertical resolution: the ERA-40 grid has twice as many levels as the grid used by Morcrette and Jakob (2000). For random overlap, the total cloud cover is strongly dependent on vertical resolution, with increasing resolution leading to more tropospheric layers and a larger cloud cover.

4.2. *Effect of horizontal structure on top-of-atmosphere CRF*

Figure 5 shows the global effects of implementing Tripleclouds. Using the plane-parallel approximation results in clouds that are too reflective in the short-wave and too emissive in the long-wave (e.g. Cahalan, *et al.*, 1994; Pomroy and Illingworth, 2000). In terms of CRF, this leads to a short-wave CRF that is too negative and a long-wave CRF that is too positive. The horizontal CRF shift introduced by Tripleclouds acts in the opposite direction to the plane-parallel biases in both spectral regions. Horizontal short-wave CRF shifts are found to be most substantial simply where clouds are present, with the largest shifts in the short-wave found off the western coasts of Africa, North America and South America, where marine stratocumulus is dominant. This is unsurprising, as marine stratocumulus covers vast areas of ocean. They have a high cloud fraction and, on account of their midlatitude location, high insolation is implied, leading to a large radiative impact (Oreopoulos, *et al.*, 2009). The long-wave horizontal CRF shift of marine stratocumulus is found to be much smaller in magnitude. The largest long-wave horizontal CRF shifts occur in the tropical western Pacific, where deep convection is prevalent. As the emission of long-wave radiation decreases with temperature, boundary-layer clouds have a much lower positive CRF than upper-tropospheric clouds, as their temperatures are much closer to that of the surface.

The magnitudes of the short-wave and long-wave CRF shifts are approximately equal in the tropical western Pacific, and hence the shift in net CRF in this location is found to be small. Elsewhere, the change in short-wave CRF dominates the net CRF shift, with the largest shifts in the regions of marine stratocumulus. The positive mean global short-wave shift of $6.15\,W\,m^{-2}$ is found to be about three times greater in magnitude than the negative mean global long-wave shift of $2.02\,W\,m^{-2}$. The short-wave shift is comparable in magnitude to the $4.2\,W\,m^{-2}$ short-wave plane-parallel bias found by Oreopoulos, *et al.* (2009) in their analysis of cloud data from MODIS. The global mean net CRF shift is $4.13\,W\,m^{-2}$, but with net shifts of up to $10\,W\,m^{-2}$ that could certainly have a sizeable radiative impact on a climate

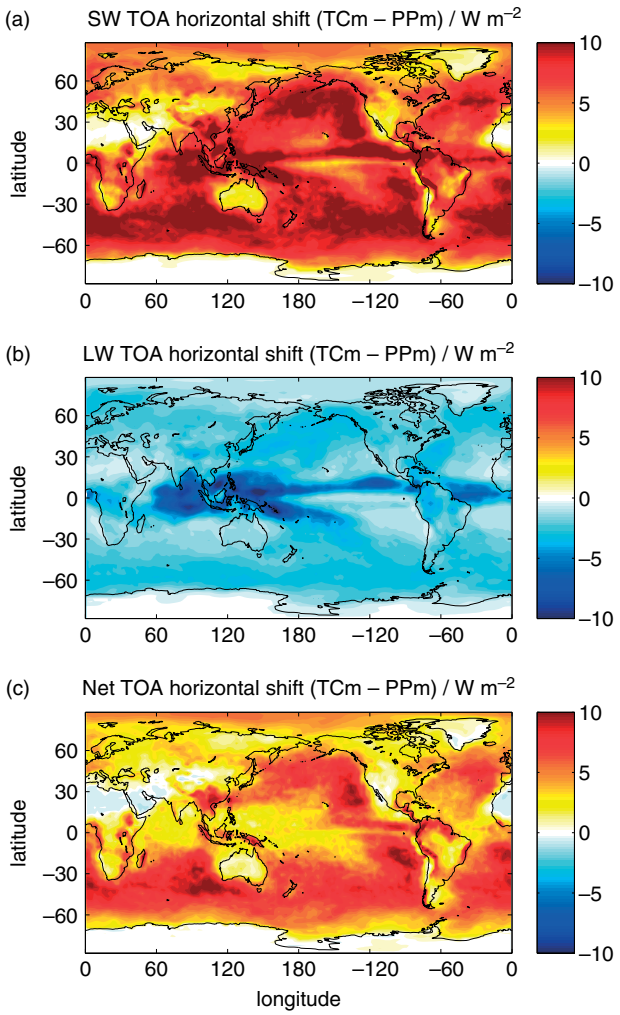

Figure 5. Global distribution of the top-of-atmosphere 'horizontal CRF shift' (the difference in cloud radiative forcing when horizontal inhomogeneity is represented using Tripleclouds as opposed to the plane-parallel approximation; TCm minus PPm). Overlap is fixed as maximum-random for (a) short-wave, (b) long-wave and (c) net CRF shifts (all W m^{-2}).

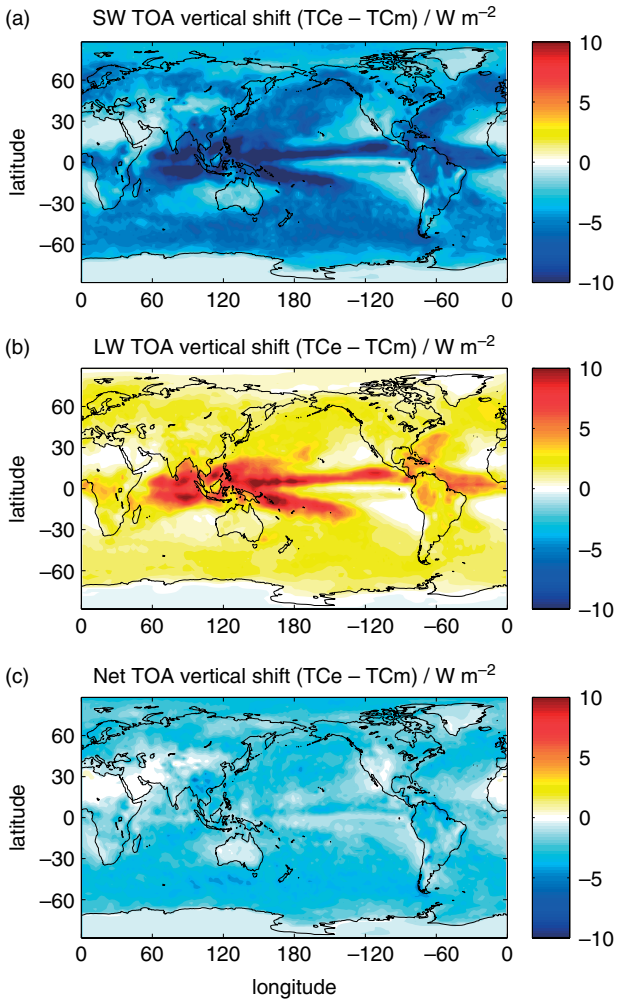

Figure 6. Global distribution of the top-of-atmosphere 'vertical CRF shift' (the difference in cloud radiative forcing when vertical overlap is represented using exponential-random overlap as opposed to maximum-random overlap; TCe minus TCm). Horizontal structure is fixed as Tripleclouds for (a) short-wave, (b) long-wave and (c) net CRF shifts (all W m^{-2}).

simulation. The uncertainty on these shifts, indicated by the error bars in Figure 9 and Table III, are quite large (of order 2 to 4 W m^{-2}; up to 100% of the mean shift). This shows that the uncertainty in our f_w value can have significant impacts on the magnitude of the horizontal shift.

4.3. *Effect of vertical structure on top-of-atmosphere CRF*

The global distribution of vertical CRF shifts introduced by replacing maximum-random overlap with exponential-random overlap for a Tripleclouds representation is shown in Figure 6. Vertical shifts are found to be of opposite sign to horizontal shifts, with the largest values found in the Tropics. This is true for both the short-wave and long-wave, although the long-wave shifts are again smaller in magnitude than the short-wave shifts by around a factor of 2 (1.98 W m^{-2} as opposed to 3.86 W m^{-2}), resulting in a negative shift in net CRF of magnitude 1.88 W m^{-2}. While the areas of deep, tropical convection give large values of vertical short-wave and long-wave CRF shift, cancellation again occurs, leaving a pattern of net vertical CRF shift that is fairly uniform.

These results show that overlap is most important in the areas of deep, tropical convection. Under such conditions, when cloud cover is less than 1 and clouds extend through many vertical layers of a gridbox, any change in overlap assumption can quickly have large effects on the cloud cover. In contrast, the regions of marine stratocumulus that were associated with the largest horizontal CRF shifts have very small vertical CRF shifts on account of their much smaller vertical extent.

In terms of the error bars, we find that the uncertainty in decorrelation height has a much smaller radiative impact than the uncertainty in f_w, with errors of much less than 1 W m^{-2} and less than 25% of the mean vertical shift. This indicates that the exact nature of the latitude fit presented in (2) would have little effect on radiation budget, and hence its crude nature is not necessarily a significant issue. A similar result was found by Barker (2008). He found minimal differences in TOA CRF when replacing exact decorrelation heights with a fixed global value.

4.4. *Total effect of cloud structure on top-of-atmosphere CRF*

The combined radiative effects on the atmosphere of Tripleclouds and exponential-random overlap can be summarised by the total net CRF shifts in Figure 7(c).

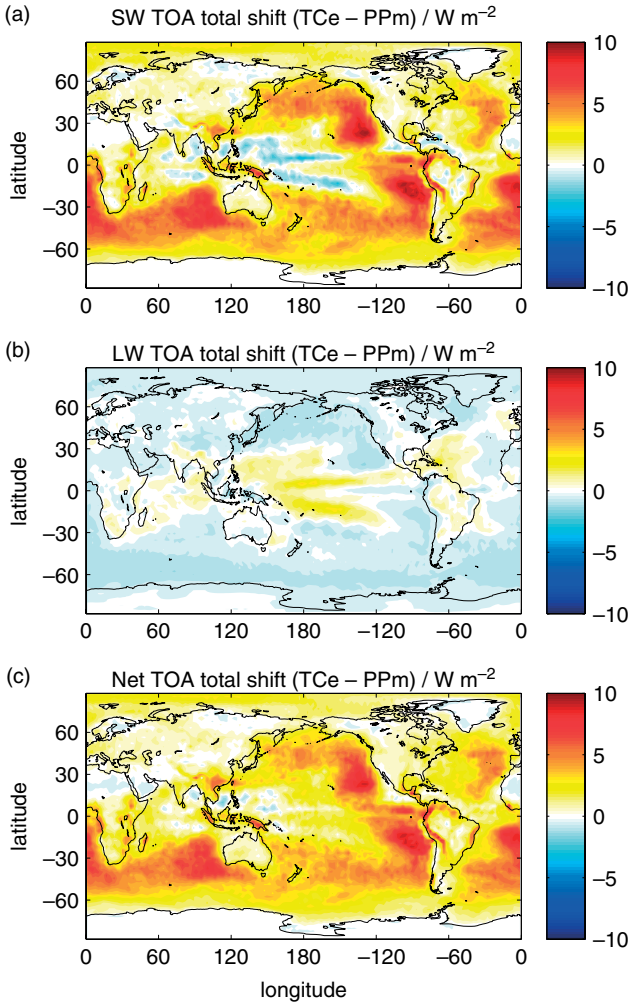

Figure 7. Global distribution of the total shift in top-of-atmosphere cloud radiative forcing when the horizontal inhomogeneity and vertical overlap schemes of the Tripleclouds schemes are implemented (TCe minus PPm): (a) short-wave, (b) long-wave and (c) net CRF (all W m^{-2}).

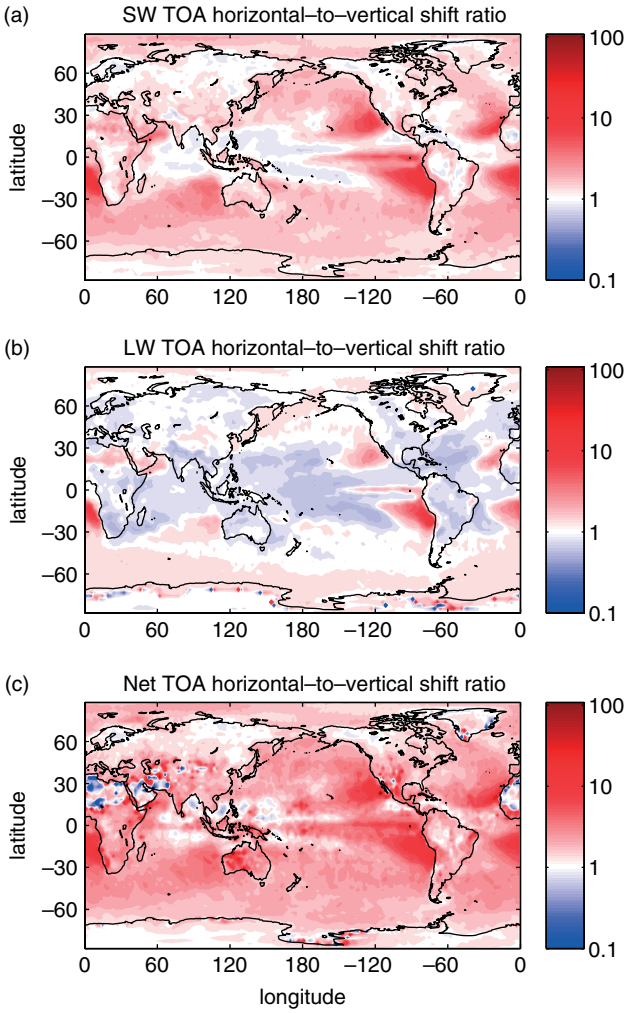

Figure 8. Global distribution of the ratio of mean magnitude of horizontal CRF shift to that of vertical CRF shift (defined in Eq. 4) on a logarithmic scale, calculated for the year of ERA-40 data, for (a) short-wave, (b) long-wave and (c) net CRF shifts. Values above 1 (red shading) indicate that horizontal CRF shifts dominate and horizontal inhomogeneity is more significant; values below 1 (blue shading) indicate that vertical CRF shifts dominate and vertical overlap is more significant.

It is worth noting that, while the global mean net CRF shift is just over 2 W m^{-2}, the shifts of 10 W m^{-2} in the areas of marine stratocumulus are significant and, in a climate simulation, would impact on heating rate and surface fluxes, which could in turn affect cloud evolution.

The short-wave and long-wave components are shown separately in Figure 7. On account of the alternate signs of the two CRF shifts, the vertical CRF shift acts to offset the horizontal CRF shift, in agreement with Hogan and Kew (2005). Cancellation is not exact, however: in most locations, the horizontal shifts are larger, but there are a few regions where vertical shifts dominate. For the regions of marine stratocumulus, the horizontal shifts dominate in the short-wave, giving an overall positive shift in net CRF. In the areas of deep, tropical convection, however, the vertical shifts dominate, with total shifts of opposite sign in both the long-wave and the short-wave. In terms of net CRF, the horizontal shifts remain dominant in most locations.

Table III shows that the global mean percentage CRF shift introduced by the full scheme is of magnitude 2.29 W m^{-2} in the short-wave and 0.04 W m^{-2} in the long-wave, again with alternate sign. This also demonstrates that the shifts in CRF caused by improved representation of horizontal inhomogeneity tend to be larger than those caused by inclusion of vertical overlap. Figure 10 shows the zonally averaged values of the mean short-wave, long-wave and net CRF for the three different cloud representations. It is seen from the position of the lines that the horizontal and vertical shifts are of opposite sign, and that the horizontal shifts are greater in magnitude.

The ratio of the mean magnitude of the horizontal CRF shift to that of the vertical CRF shift is plotted as a global distribution in Figure 8; in other words:

$$\text{ratio} = \frac{|\text{CRF(TCm)} - \text{CRF(PPm)}|}{|\text{CRF(TCe)} - \text{CRF(TCm)}|} . \qquad (4)$$

In agreement with Figures 9 and 10, the effect of representing inhomogeneity seems to have a far more significant effect on the radiation budget than improving overlap. This is particularly true in both spectral regions in areas of marine stratocumulus, where overlap is largely irrelevant. In the Tropics, however, the two effects are seen to be of comparable size in the short-wave, implying the approximate cancellation of CRF shifts shown in the previous section. In the long-wave, the vertical effects are seen to dominate, particularly in the Tropics, where deep convection tends to occur. The clouds used by Barker, *et al.*

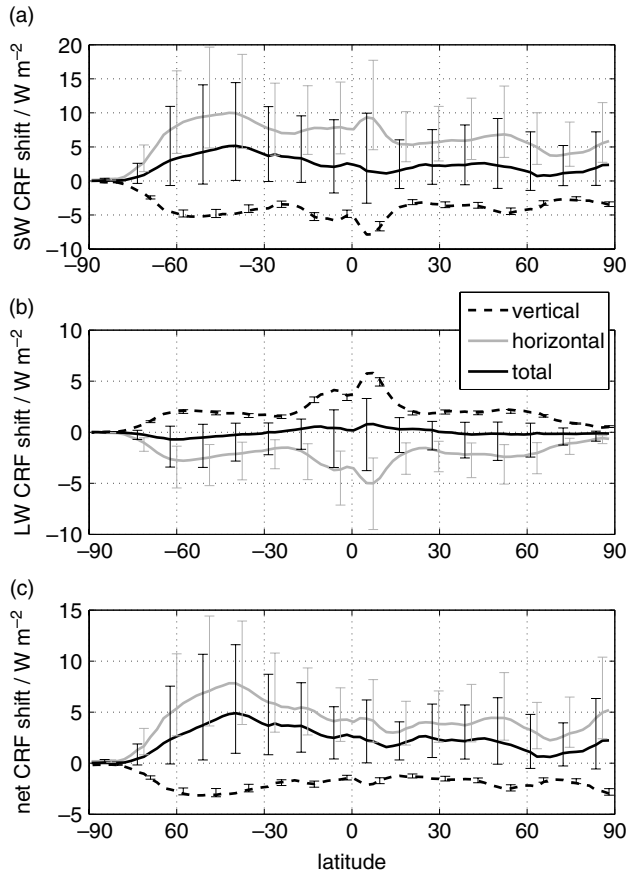

Figure 9. Variation of zonal mean values of (a) short-wave, (b) long-wave and (c) net top-of-atmosphere shifts for the year of ERA-40 data. The error bars indicate the effects of the uncertainty in the Tripleclouds and exponential-random parametrization on the radiative transfer.

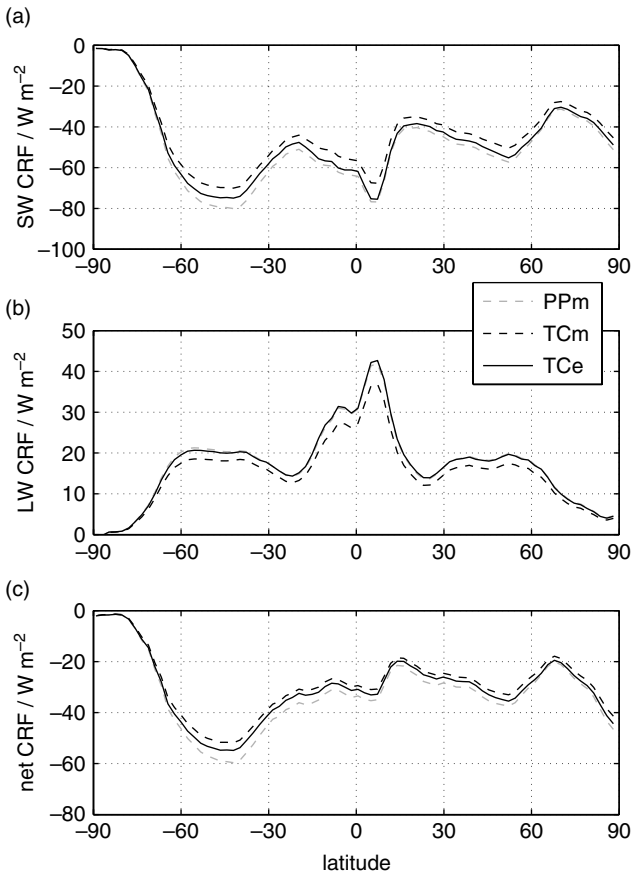

Figure 10. Variation of zonal mean values of (a) short-wave, (b) long-wave and (c) net top-of-atmosphere cloud radiative forcing (CRF) with latitude. CRFs calculated from the year of ERA-40 are shown for the three cloud schemes.

(1999) to compare the effects of representing horizontal inhomogeneity and vertical overlap were generated using a cloud-resolving model and a scenario set up from scenes of tropical convection. For tropical clouds in our investigation, we also find that the two components of cloud structure had effects of similar magnitude, indicating agreement between our results and those of Barker, *et al.* (1999).

It is apparent from the results of this section that either representing horizontal inhomogeneity or improving the overlap scheme in a plane-parallel, maximum-random cloud scheme, without the other, is insufficient. Figure 9 implies clearly that fixing overlap alone in a PPm scheme would cause the CRF biases to become larger, while fixing inhomogeneity alone changes the CRFs in the correct direction, but with an overcompensation, resulting in a bias of the opposite sign and about half the magnitude. Hence, as both components of cloud structure have sizeable impacts on radiation budget, it is apparent that representing horizontal inhomogeneity and vertical overlap are equally important.

4.5. *Effect of structure on surface CRF*

The distributions of surface CRF shifts (not shown) are similar to those at the TOA, with a few differences. In the short-wave, the magnitudes of both the horizontal and vertical CRF shifts are larger at the surface by about 3 W m^{-2}. This results in a very small total short-wave shift of less than 1 W m^{-2} when averaged globally. The patterns of the short-wave shifts at the surface are very similar to those at the top of the atmosphere, with largest horizontal shifts in marine stratocumulus and largest vertical shifts in deep, tropical convection.

In the long-wave, there are some notable differences in the patterns of the CRF shifts, most of which are attributable to the differences in radiation budget between surface and TOA. The regions of high horizontal TOA CRF shift in the areas of deep, tropical convection are found to be absent at the surface. Instead, the highest regions of horizontal shift are at higher latitudes, most notably in the storm tracks and marine stratocumulus areas, where the CRF shift reaches 10 W m^{-2} in magnitude locally. The surface CRF of a low-level cloud is much more positive than a high-level cloud, on account of its higher temperature. Therefore, any changes affecting low-level clouds will have a much larger impact on long-wave surface radiation budget than those affecting high clouds. Hence, the largest horizontal shifts are seen where inhomogeneous low clouds exist. Long-wave vertical CRF shifts are seen to be largest at the surface in locations where clouds have low bases but have a larger vertical extent. This leads to sizeable shifts in the storm tracks, but markedly smaller shifts in the areas of deep, tropical convection.

The smaller magnitude of both the horizontal and vertical long-wave CRF shift at the surface for areas of deep, tropical convection are found to combine to have little effect in the total shift patterns. The total net CRF shift at the surface is found to be similar to that at the top of the atmosphere, but with a reduction in shift in areas

of marine stratocumulus (about 5 W m^{-2}; half the size of the corresponding TOA shift). Table III shows that, at the surface, both the short-wave and long-wave total shifts are larger in magnitude than at the TOA, but the net total shift is smaller.

5. Summary and conclusions

In this paper, we have quantified the effect of cloud structure on the global radiation budget, and also compared the individual radiative effects of horizontal and vertical cloud structure representations. Three different cloud representations were applied to a year of ERA-40 re-analysis data and radiative transfer calculations performed using the Edwards–Slingo code. The radiative performance of the cloud representations was evaluated in terms of cloud radiative forcing (CRF). First, the CRFs calculated using 'Tripleclouds' with 'exponential-random' overlap (TCe) and the plane-parallel, maximum-random scheme (PPm) were compared with CRF data from the Clouds and the Earth's Radiant Energy System (CERES) project to verify that the calculated CRFs were realistic. Both patterns and magnitudes of short-wave and long-wave CRFs were found to be comparable, although there were a few local and systematic differences that were attributed to the difference between the modelled clouds from ERA-40 and the clouds observed by satellite as part of CERES and the CERES definition of clear-sky fluxes.

The global radiative effects of introducing horizontal inhomogeneity (the 'horizontal shift') and of improving the representation of vertical overlap (the 'vertical shift') were then considered at the TOA. In the short-wave, horizontal CRF shifts were found to be largest in areas of marine stratocumulus, which cover large areas of the ocean and are radiatively important. Long-wave horizontal CRF shifts were found to be largest in regions of deep, tropical convection, where the long-wave CRFs are largest on account of the height of the clouds. These two shifts are of opposite sign, and it turns out that the two shifts cancel in the deep, tropical convection, giving a near-zero result. In areas of marine stratocumulus, however, the horizontal shifts are still strongly positive, with a global mean shift of 4.13 W m^{-2}.

Vertical TOA CRF shifts were found to be of opposite sign to the horizontal CRF shifts and were largest in the short-wave and long-wave where the prevalent clouds are tallest: namely, in areas of deep, tropical convection. In net CRF shift terms, however, these are found again to be of similar magnitude, with a small negative shift found in most locations and a global mean vertical shift of –1.88 W m^{-2}.

The combined effect of these two shifts is that they offset each another. The total net CRF shift is found to be near zero in deep, tropical convection, but sizeably positive in areas of marine stratocumulus. The global mean total net CRF shift was found to be 2.25 W m^{-2}; which may not seem a large effect, but it should be noted that the shifts of order 10 W m^{-2} in marine stratocumulus areas could certainly cause impacts on cloud life cycles in climate simulations.

Investigations into the effect of the uncertainty in our parametrization on the horizontal and vertical shifts revealed that the uncertainty in fractional standard deviation of water content f_w has a much larger effect on the horizontal shifts than the uncertainty in decorrelation height $Z_{0\beta}$ has on the vertical shifts, with the spread in the total combined shift being dominated by the effect of the uncertainty in f_w. This implies that the crudeness of our linear latitude dependence of $Z_{0\beta}$, described in Part I, is not necessarily an issue, as the CRF shifts are relatively insensitive to its values. In contrast, however, it shows that the uncertainty in f_w is much more important, and that more work is required to determine its values with greater accuracy.

While the representation of horizontal inhomogeneity in a GCM may have a larger impact on the radiation budget than improving the representation of vertical overlap, it turns out that both are important, as correcting one and not the other can increase the error in CRF. Fixing horizontal inhomogeneity and not vertical overlap can result in overcompensation, and fixing vertical overlap and not horizontal inhomogeneity can result in biases of larger magnitude. In other words, improving representations of both horizontal inhomogeneity and vertical overlap are imperative to create improvements in radiation budget. We are currently implementing Tripleclouds and exponential-random overlap into the Met Office Unified Model to evaluate the performance of the two components in terms of their effects on future climate.

Acknowledgements

We thank Richard Allan for assistance with the CERES data and Paul Berrisford for support with ERA-40 data. Also Keith Shine and Jean-Jacques Morcrette are thanked for their thoughts and input. This research was funded by the University of Reading via a Research Endowment Trust Fund (RETF) studentship and NERC grant NE/F011261/1.

References

Allan RP, Ringer MA. 2003. Inconsistencies between satellite estimates of long-wave cloud radiative forcing and dynamical fields from re-analyses. *Geophys. Res. Lett.* **30**: DOI: 10.1029/2003GL017019.

Allan RP, Ringer MA, Pamment JA, Slingo A. 2004. Simulation of the Earth's radiation budget by the European Centre for Medium-Range Weather Forecasts 40-year reanalysis (ERA-40). *J. Geophys. Res.* **109**: DOI: 10.1029/2004JD004816.

Barker HW. 2008. Representing cloud overlap with an effective decorrelation length: An assessment using CloudSat and CALIPSO data. *J. Geophys. Res.* **113**: DOI: 10.1029/2008JD010391.

Barker HW, Stephens GL, Fu Q. 1999. The sensitivity of domain-averaged solar fluxes to assumptions about cloud geometry. *Q. J. R. Meteorol. Soc.* **125**: 2127–2152.

Bender FA, Rodhe H, Charlson RJ, Ekman AML, Loeb N. 2006. 22 views of the global albedo – Comparison between 20 GCMs and two satellites. *Tellus A* **58**: 320–330.

Cahalan RF, Ridgway W, Wiscombe WJ, Bell TL, Snyder JB. 1994. The albedo of fractal stratocumulus clouds. *J. Atmos. Sci.* **51**: 2434–2455.

Carlin B, Fu Q, Lohmann U, Mace GG, Sassen K, Comstock JM. 2002. High-cloud horizontal inhomogeneity and solar albedo bias. *J. Climate* **15**: 2321–2339.

Chevallier F, Bauer P, Kelly G, Jakob C, McNally T. 2001. Model clouds over oceans as seen from space: Comparison with HIRS/2 and MSU radiances. *J. Climate* **14**: 4216–4229.

Edwards JM, Slingo A. 1996. Studies with a flexible new radiation code. I: Choosing a configuration for a large-scale model. *Q. J. R. Meteorol. Soc.* **122**: 689–719.

Hogan RJ, Illingworth AJ. 2000. Deriving cloud overlap statistics from radar. *Q. J. R. Meteorol. Soc.* **126**: 2903–2909.

Hogan RJ, Kew SF. 2005. A 3D stochastic cloud model for investigating the radiative properties of inhomogeneous cirrus clouds. *Q. J. R. Meteorol. Soc.* **131**: 2585–2608.

Illingworth AJ, Hogan RJ, O'Connor EJ, Bouniol D, Brooks ME, Delanoë J, Donovan DP, Eastment JD, Gaussiat N, Goddard JWF, Haeffelin M, Klein Baltink H, Krasnov OA, Pelon J, Piriou J-M, Protat A, Russchenberg HWJ, Seifert A, Tompkins AM, Van Zadelhoff G-J, Vinit F, Willén U, Wilson DR, Wrench CL. 2007. Cloudnet – Continuous evaluation of cloud profiles in seven

operational models using ground-based observations. *Bull. Amer. Meteorol. Soc.* **88**: 883–898.

Kristjánsson JE, Edwards JM, Mitchell DL. 2000. Impact of a new scheme for optical properties of ice crystals on climates of two GCMs. *J. Geophys. Res.* **105**: 10063–10079.

Mace GG, Benson-Troth S. 2002. Cloud-layer overlap characteristics derived from long-term cloud radar data. *J. Climate* **15**: 2505–2515.

McClatchey RA, Fenn RW, Selby JEA, Volz FE, Garing JS. 1972. Optical properties of the atmosphere. Report number AFCRL72-0497. Air Force Cambridge Research Laboratories, Bedford, Massachusetts, USA.

Morcrette J, Jakob C. 2000. The response of the ECMWF model to changes in the cloud overlap assumption. *Mon. Weather Rev.* **128**: 1707–1732.

Oreopoulos L, Platnick S, Hong G, Yang P, Cahalan RF. 2009. The shortwave radiative forcing bias of liquid and ice clouds from MODIS observations. *Atmos. Chem. Phys.* **9**: 5865–5875.

Pomroy HR, Illingworth AJ. 2000. Ice cloud inhomogeneity: Quantifying bias in emissivity from radar observations. *Geophys. Res. Lett.* **27**: 2101–2104.

Räisänen P, Barker HW, Khairoutdinov MF, Li J, Randall DA. 2004. Stochastic generation of sub-gridscale cloudy columns for large-scale models. *Q. J. R. Meteorol. Soc.* **130**: 2047–2067.

Randall DA, Wood RA, Bony S, Colman R, Fichefet T, Fyfe J, Kattsov V, Pitman A, Shukla J, Srinivasan J, Stouffer RJ, Sumi A, Taylor KE. 2007. Climate models and their evaluation. Chapter 8 in *Climate Change 2007: the Physical Science Basis.* Contribution of Working Group I to the Fourth Assessment Report of the Itergovernmental Panel on Climate Change. Solomon S, Qin D, Manning M, Chen Z, Marquis M, Averyt KB, Tignor M, Miller HL. (eds.) Cambridge University Press: Cambridge, UK.

Shonk JKP, Hogan RJ. 2008. Tripleclouds: An efficient method for representing cloud inhomogeneity in 1D radiation schemes by using three regions at each height. *J. Climate* **21**: 2352–2370.

Shonk JKP, Hogan RJ, Edwards JM, Mace GG. 2010. Effect of improving representation of horizontal and vertical cloud structure on the Earth's global radiation budget. Part I: Review and parametrization. *Q. J. R. Meteorol. Soc.* **136**: 1191–1204, DOI: 10.1002/qj.647.

Slingo A. 1990. Sensitivity of the Earth's radiation budget to changes in low clouds. *Nature* **343**: 49–51.

Tompkins AM. 2002. A prognostic parametrisation for the subgrid-scale variability of water vapour and clouds in large-scale models and its use to diagnose cloud cover. *J. Atmos. Sci.* **59**: 1917–1942.

Uppala SM, Kållberg PW, Simmons AJ, Andrae U, Da Costa Bechtold V, Fiorino M, Gibson JK, Haseler J, Hernandez A, Kelly GA, Li X, Onogi K, Saarinen S, Sokka N, Allan RP, Andersson E, Arpe K, Balmaseda MA, Beljaars ACM, Van De Berg L, Bidlot J, Bormann N, Caires S, Chevallier F, Dethof A, Dragosavac M, Fisher M, Fuentes M, Hagemann S, Hólm E, Hoskins BJ, Isaksen L, Janssen PAEM, Jenne R, McNally AP, Mahfouf JF, Morcrette J-J, Rayner NA, Saunders RW, Simon P, Sterl A, Trenberth KE, Untch A, Vasiljevic D, Viterbo P, Woollen J. 2005. The ERA-40 re-analysis, *Q. J. R. Meteorol. Soc.* **131**: 2961–3012.

Wielicki BA, Barkstrom BR, Harrison EF, Lee III RB, Louis Smith G, Cooper JE. 1996. Clouds and the Earth's Radiant Energy System (CERES): An Earth observing system experiment. *Bull. Amer. Meteorol. Soc.* **77**: 853–868.

